nature biotechnology

# Efficiency of siRNA delivery by lipid nanoparticles is limited by endocytic recycling

Gaurav Sahay[1], William Querbes[2], Christopher Alabi[3], Ahmed Eltoukhy[3], Sovan Sarkar[4], Christopher Zurenko[2], Emmanouil Karagiannis[1], Kevin Love[1,3], Delai Chen[1], Roberto Zoncu[4], Yosef Buganim[4], Avi Schroeder[1,3], Robert Langer[1,3,5,6] & Daniel G Anderson[1,3,5,6]

**Despite efforts to understand the interactions between nanoparticles and cells, the cellular processes that determine the efficiency of intracellular drug delivery remain unclear. Here we examine cellular uptake of short interfering RNA (siRNA) delivered in lipid nanoparticles (LNPs) using cellular trafficking probes in combination with automated high-throughput confocal microscopy. We also employed defined perturbations of cellular pathways paired with systems biology approaches to uncover protein-protein and protein–small molecule interactions. We show that multiple cell signaling effectors are required for initial cellular entry of LNPs through macropinocytosis, including proton pumps, mTOR and cathepsins. siRNA delivery is substantially reduced as ≅70% of the internalized siRNA undergoes exocytosis through egress of LNPs from late endosomes/lysosomes. Niemann-Pick type C1 (NPC1) is shown to be an important regulator of the major recycling pathways of LNP-delivered siRNAs. NPC1-deficient cells show enhanced cellular retention of LNPs inside late endosomes and lysosomes, and increased gene silencing of the target gene. Our data suggest that siRNA delivery efficiency might be improved by designing delivery vehicles that can escape the recycling pathways.**



siRNAs are a potential new class of medicines that can selectively silence disease-causing genes[1–3]. LNPs are the most advanced siRNA delivery system to date, having recently shown therapeutic efficacy in clinical trials[4]. Although efforts to define the physicochemical properties of nanoparticles that contribute to efficient cellular delivery are ongoing, the cellular factors that regulate nanoparticle-mediated siRNA delivery remain largely unclear[5–7].

Nanoparticles utilize different endocytosis pathways for cellular entry[5]. Intracellular trafficking of nanoparticles is a dynamic process, through which macromolecules are transported to different subcellular destinations, with the majority of material targeted to the lysosomes for degradation[5]. It has been hypothesized that the buffering capacity of nanoparticles activates the proton pump that raises osmotic pressure inside an endosome, resulting in its swelling and subsequent escape of siRNA from the endosome[7,8]. Alternatively, it has been suggested that cationic lipids in LNPs interact with anionic lipids of the endosome, causing destabilization of the endosomal membrane[9]. Regardless of the release mechanism, imaging studies have shown that nucleic acids are largely trapped inside the endosomes and lysosomes with only a small fraction being released to the cytoplasm[10–12]. Endosomal transport requires multiple heterotypic or homotypic endocytic fusion events with a constantly changing vesicular milieu regulated by a diverse set of endosomal proteins and different cell signaling cascades[13,14]. The effect of this interplay between cell signaling and endocytosis on LNP trafficking needs to be further defined.

In this study, we used automated, high-resolution microscopy to screen a library of small molecules that have a range of effects on cell signaling, endocytosis and autophagy, and identify important key regulators of cellular uptake of cationic LNPs that can encapsulate siRNA (**Supplementary Data**). These LNPs were formed by the complexation of siRNA with the cationic lipid C12-200. They were further formulated with different excipients using a previously reported microfluidic process that generates slightly positively charged nanoparticles (~70–80 nm in size)[15]. They have demonstrated unprecedented efficacy in the delivery of siRNA *in vivo*[16,17]. The potency of this delivery system, tested in rodents and nonhuman primates, is in a range similar to that of LNPs at the forefront of clinical trials[4]. In rodents, no liver toxicity was observed at 1 mg/kg, a dose 100-fold above the efficacious range of silencing[16].

When we incubated HeLa-GFP cells with LNPs containing Alexa Fluor 647–labeled siRNA against GFP (siAF647-GFP) for 3 h, the particles appeared to localize at the perinuclear region within 1 h after exposure (**Supplementary Fig. 1a**,**b**). Subcellular localization of LNP-siRNA in the presence of small-molecule inhibitors under similar conditions was visualized and the amount of internalized siRNA was quantified. The small-molecule library consisted of molecules that affect cell signaling and intracellular trafficking and that either induce or inhibit autophagy (for a list of the inhibitors used and the quantification

[1]The David H. Koch Institute for Integrative Cancer Research, Massachusetts Institute of Technology, Cambridge, Massachusetts, USA. [2]Alnylam Pharmaceuticals, Cambridge, Massachusetts, USA. [3]Department of Chemical Engineering, Massachusetts Institute of Technology, Cambridge, Massachusetts, USA. [4]Whitehead Institute for Biomedical Research, Massachusetts Institute of Technology, Cambridge, Massachusetts, USA. [5]Harvard-MIT Division of Health Science and Technology, Massachusetts Institute of Technology, Cambridge, Massachusetts, USA. [6]Institute for Medical Engineering and Science, Cambridge, Massachusetts, USA. Correspondence should be addressed to D.G.A. (dgander@mit.edu).

Received 13 January; accepted 17 May; published online 23 June 2013; doi:10.1038/nbt.2614

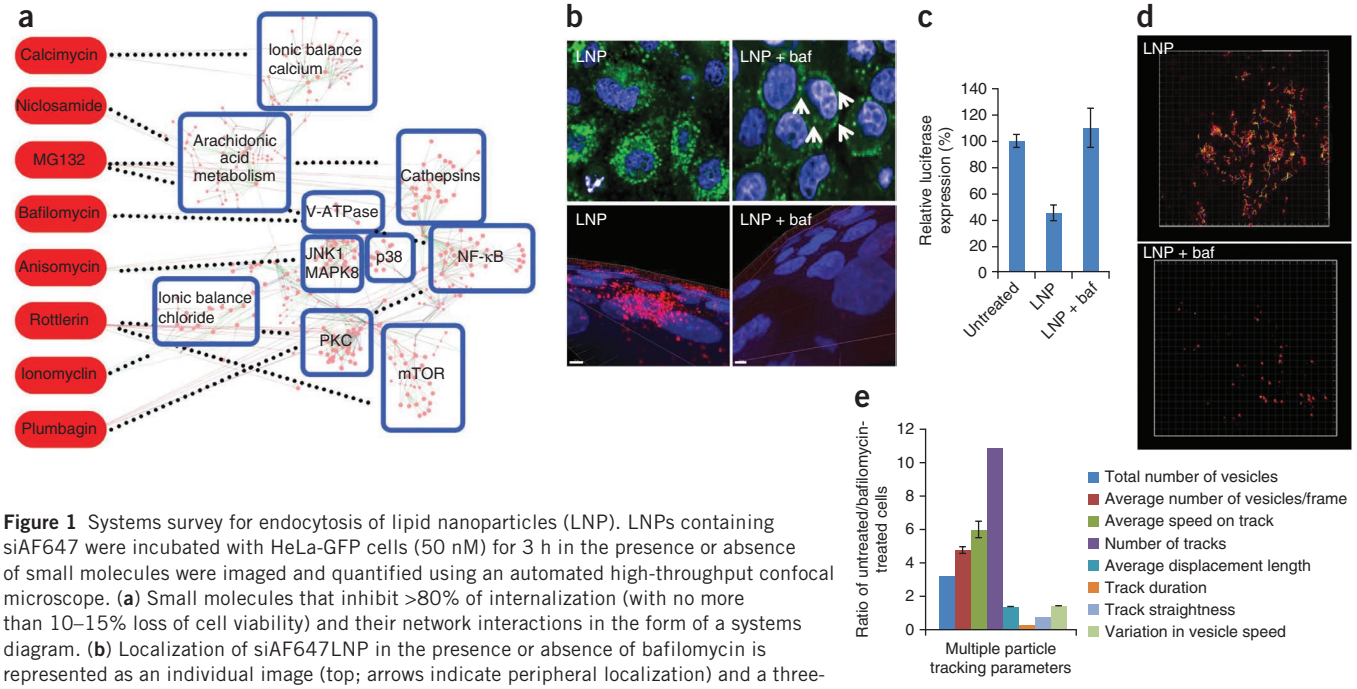


**Figure 1** Systems survey for endocytosis of lipid nanoparticles (LNP). LNPs containing siAF647 were incubated with HeLa-GFP cells (50 nM) for 3 h in the presence or absence of small molecules were imaged and quantified using an automated high-throughput confocal microscope. (**a**) Small molecules that inhibit >80% of internalization (with no more than 10–15% loss of cell viability) and their network interactions in the form of a systems diagram. (**b**) Localization of siAF647LNP in the presence or absence of bafilomycin is represented as an individual image (top; arrows indicate peripheral localization) and a three-dimensional z-stack (bottom). Scale bars, LNP: 70 μm and LNP+baf: 100 μm). (**c**) Dual HeLa cells were exposed to LNP (siLuc, 10 nM) in the presence or absence of bafilomycin (1 μM). Luciferase to Renilla levels were measured for silencing activity. Experiments were done in triplicate; errors are plotted as s.e.m. (**d**,**e**). Time-lapse TIRF microscopy of cells exposed to siAF647-LNPs (50 nM, 3 h) in the presence or absence of bafilomycin combined with multiple particle tracking (MPT). A snapshot of vesicular tracks indicating the movement of LNPs in the presence or absence of bafilomycin (**d**). The ratio between the MPT parameters for untreated and/or bafilomycin-treated cells was calculated to provide a quantitative measure of differences in LNP trafficking with or without bafilomycin (**e**). Errors of ratios are plotted through propagation of errors from division.

of their effect on LNP uptake, see **Supplementary Data**). We considered the subset of small molecules that substantially inhibited LNP uptake, and using databases, identified the proteins with which the small molecules interact, and created protein-protein and protein–small molecule interaction networks. This systems analysis identified several endocytic regulators required for LNP entry, which includes $V_o$-ATPase, mTOR (mammalian target of rapamycin), cathepsins, protein kinase C, NFκB, calcium channels, chloride channels and constituents of arachidonic acid metabolic pathways (**Fig. 1a**).

Previous work has identified signaling cascades involving mTOR and cathepsins, among others, as regulators of the cellular uptake of glucose and viruses by macropinocytosis[18,19]. We have summarized these effectors that affect cellular trafficking of LNPs in **Supplementary Table 1**. Previous studies have shown that interference with acidification affects release of nucleic acids from endosomal compartments[20], and our results further corroborated the effects of proton pumps on endocytosis of LNPs. We found that the $V_o$-ATPase inhibitor, bafilomycin, inhibited LNP entry into cells (**Fig. 1b**) whereas it had no effect on the LNPs' stability (**Supplementary Fig. 2a**). Both LNPs with different cationic lipid compositions containing siRNA and liposomes composed of hydrogenated soybean phosphatidylcholine containing small molecules showed a marked decrease in uptake into cells in the presence of two different proton pump inhibitors, concanamycin and bafilomycin (**Supplementary Fig. 2b**,**c**)[21]. Furthermore, treatment with bafilomycin led to a decrease in siRNA-induced target-gene silencing (**Fig. 1c**).

We further investigated the interactions of the LNPs with the cell membrane in the presence or absence of bafilomycin using time-lapse total internal reflection fluorescence (TIRF) microscopy, which allows high-resolution imaging at the cell surface. Multiple particle tracking revealed that LNP-containing vesicles moved, on average, six times faster in untreated cells than in bafilomycin-treated cells. After bafilomycin treatment endosomes also appeared to form in substantially lower numbers (67% reduction) and had a slower rate of disappearance (increased track duration) from the focal plane (**Fig. 1d**,**e** and **Supplementary Movies 1** and **2**). Seventy-five percent reduction of LNP-containing vesicles per frame were observed after bafilomycin treatment, and those that formed got enlarged owing to a block in the transport of early endosomes to late endosome/lysosomes (as has been previously reported[22]).

To identify internalization pathways that are required for cationic LNP entry into cells, we depleted key endocytic regulators using siRNA in HeLa cells. Downregulation of Cdc42 and Rac1 (regulators of macropinocytosis) led to ~80% decrease in LNP uptake, whereas inhibition of clathrin heavy chain-1 and caveolin-1 (regulators of clathrin and caveolae, respectively, which mediate endocytosis) had little impact on LNP entry (**Fig. 2a**). Further transport of LNPs to select endocytic compartments in these cells was analyzed through co-localization studies based on endocytic markers. First, LNP initial entry through macropinocytosis was confirmed through strong localization with Cdc42-GFP and ovalbumin-positive vesicles (both markers for macropinocytosis) as compared to that with Arf6-GFP–positive vesicles (clathrin-and dynamin-independent pathways) (**Supplementary Fig. 3a**). Second, image-based kinetics of LNP delivery to the general endosomal and lysosomal system revealed little co-localization of LNPs with EEA1 or Rab5-RFP (early endosome markers) (after 3 h incubation, at several time points after incubation (chase), ~5–10% co-localization) but showed a steady increase in co-localization with LAMP1-, LAMP2-, Rab7-GFP- and Lysotracker-positive vesicles (late endosome and lysosome markers), starting as early as after the 15-min chase and showing a steady increase to around 50% localization with late endosomes/lysosomes

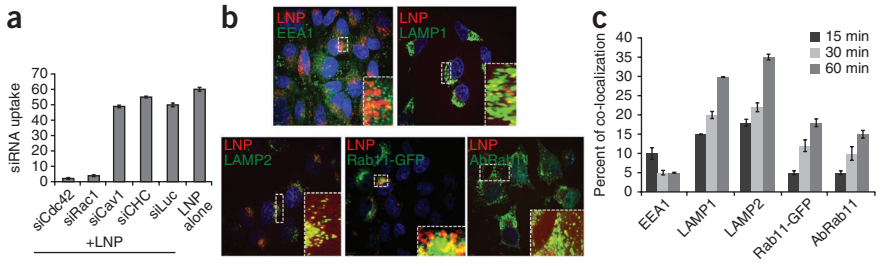


**Figure 2** Cellular trafficking of LNPs. (**a**) Quantitative image analysis of siAF647-LNP cellular uptake (3 h) in HeLa cells silenced with siRNA against key endocytic regulators (Cdc42, Rac-1, clathrin heavy chain (CHC), caveolin-1 (Cav-1)). siRNA against luciferase serves as a negative control. (**b**,**c**) Image-based quantitative analysis of siAF647-LNPs co-localization (3-h pulse; 15-, 30-, 60-min chase) with markers of endocytosis, anti-EEA1 (early endosomes), anti-LAMP1 (late endosome/lysosomes), anti-LAMP2 (late endosomes/lysosomes), Rab11-GFP and anti-Rab11 (both mark endocytic recycling compartment). High-resolution z-stack confocal images representative of 60-min chase are presented in different panels (**b**). Quantification of LNP-siRNA cellular uptake using high-throughput confocal microscopy after indicated times (**a**,**c**). Error bars, mean ± s.e.m.

after 60 min (**Fig. 2b**,**c** and **Supplementary Fig. 3b**,**c**). Notably, after 60 min a fraction of the labeled siRNA starts to show co-localization with markers of the tubulovesicular endocytic recycling compartment (Rab11-GFP, antibody against Rab-11, transferrin) whereas a decrease in localization with lysosomal positive vesicles was observed (**Fig. 2b**,**c** and **Supplementary Fig. 3c**). Inhibition of Rab11 (Rab11 siRNA and dominant negative (DN)-Rab11) to interfere with early endocytic recycling causes a 1.5-fold reduction in LNP internalization (**Supplementary Fig. 3d**,**e**). This decreased internalization may be a result of reduced endocytic recycling of trafficking regulators required for LNP entry.

Autophagy, another catabolic process that routes cytosolic proteins to the lysosomes[23,24], was apparently not involved in LNP-mediated gene silencing as LNPs showed little co-localization with markers of autophagy (**Supplementary Fig. 4a**,**b**). Autophagy-deficient cells ($Atg5^{-/-}$)[24] showed little if any differences in LNP-mediated gene silencing when compared to autophagy competent ($Atg5^{+/+}$) cells (**Supplementary Fig. 4c**).

Overall, C12-200–based cationic LNPs utilize macropinocytosis to enter cells and bypass the early endosomes; a small fraction is directed to the endocytic recycling compartment whereas most LNPs traffic toward the late endosome from where they are routed to the lysosomes. Our results are consistent with previous studies that cationic LNPs utilize distinct mechanisms of entry when compared to ionizable LNPs, which internalize through ApoE-dependent entry mechanisms[16,25].

In addition to the moderate co-localization of LNPs with endocytic recycling compartment, our imaging studies also indicated a considerable redistribution of LNPs in the presence of a wide variety of compounds from the screen that cause stress on the endoplasmic reticulum (**Supplementary Data**). Therefore, we wanted to quantify the kinetics of LNP disassembly and the relative contributions of internalization and recycling on siRNA delivery using a fluorescence resonance energy transfer (FRET) probe[26]. The probe contains two identical siRNAs, each labeled with a different fluorophore that together form a FRET pair. The siRNA-bound fluorophores aggregate with the cationic lipids in the nanoparticle mixture and undergo FRET, which is indicative of intact LNPs. Flow cytometry data showed a time-dependent decrease in FRET-based fluorescence signal within 1 h of internalization, which was indicative of LNP disassembly inside cells (**Fig. 3a**). However, the fluorescence emanating from a single fluorophore (AF647) remained constant during this time. A decline in AF647 signal was observed only after 1–4 h, which substantially diminished after 24 h. Therefore, LNPs disassembled rapidly within the first hour of entry followed by degradation or recycling of siRNA within 24 h (**Fig. 3a**). Labeled siRNA was located in vesicular compartments alongside microtubules 1 h after incubation; indicating that most siRNAs remain trapped inside endosomes after nanoparticle disassembly (**Fig. 3b**).

To show that the reduction of intracellular siRNA-linked fluorescence was due to recycling of the siRNA to the extracellular media, we measured the fluorescence in the supernatant at multiple time points

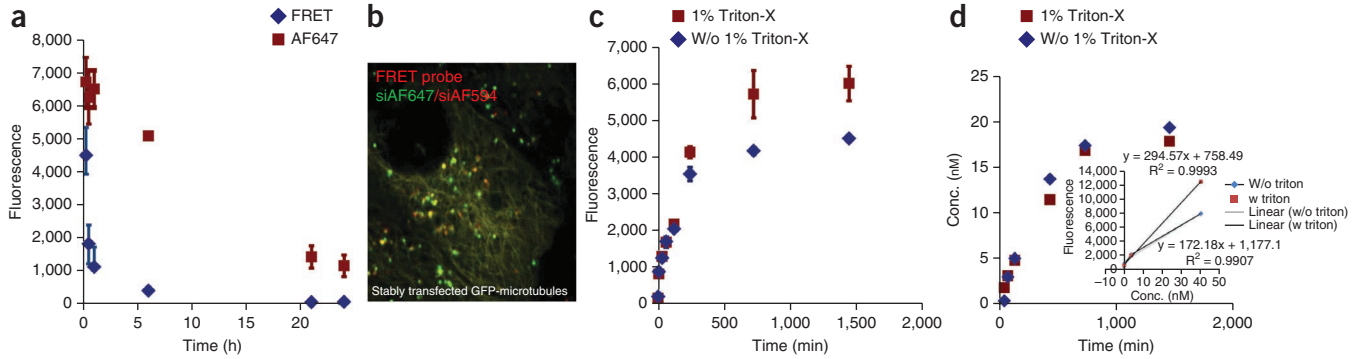


**Figure 3** Quantitative analysis for disassembly and recycling of LNPs. (**a**) HeLa cells were exposed to LNP with the FRET pair (AF647/AF594 siRNA), washed and replenished with media. Changes in FRET (excitation-561 nm, emission-641 nm) intensity were monitored at different time points using flow cytometry to quantify LNP disassembly. The emission from a single fluorophore (excitation-633 nm, emission-641 nm) was used to measure intracellular siRNA at these time points. (**b**) Cellular uptake of FRET probe-LNP (siAF647/siAF594, 3 h) was imaged in stably transfected GFP-tubulin cells 1 h after incubation. (**c**) siAF647-LNP was pulsed for 3 h, washed and incubated with fresh media to remove noninternalized particles. Media was removed at multiple time points and analyzed using a fluorescent reader to determine amount recycled. 1% Triton-X was later added (red curve) to the media and fluorescence was remeasured. (**d**) Concentration of siRNA was obtained from fluorescence values from **c** that were extrapolated using the standard curve (inset). All experiments were performed in triplicate. Error bars, mean ± s.e.m.

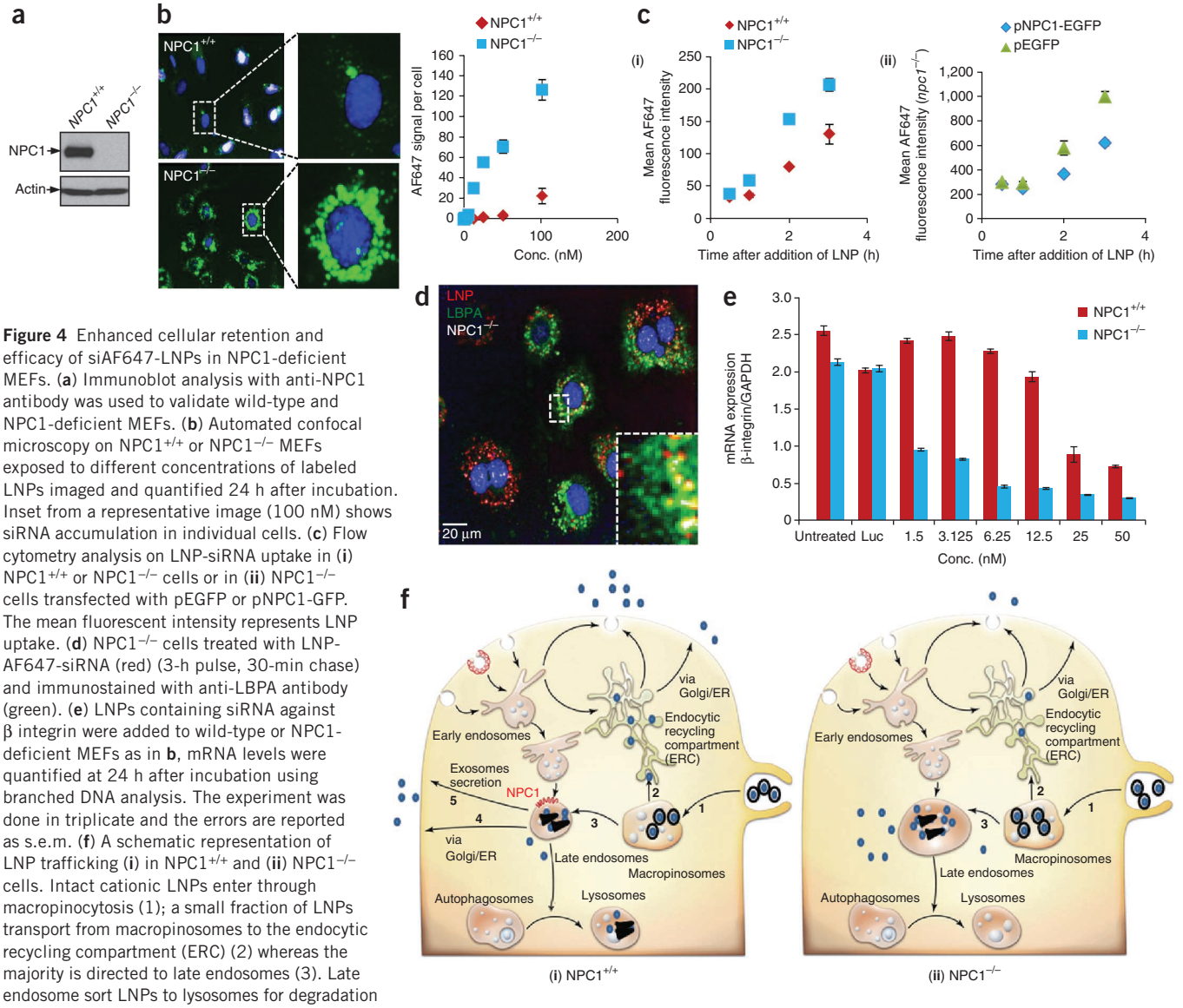


**Figure 4** Enhanced cellular retention and efficacy of siAF647-LNPs in NPC1-deficient MEFs. (**a**) Immunoblot analysis with anti-NPC1 antibody was used to validate wild-type and NPC1-deficient MEFs. (**b**) Automated confocal microscopy on NPC1$^{+/+}$ or NPC1$^{-/-}$ MEFs exposed to different concentrations of labeled LNPs imaged and quantified 24 h after incubation. Inset from a representative image (100 nM) shows siRNA accumulation in individual cells. (**c**) Flow cytometry analysis on LNP-siRNA uptake in (**i**) NPC1$^{+/+}$ or NPC1$^{-/-}$ cells or in (**ii**) NPC1$^{-/-}$ cells transfected with pEGFP or pNPC1-GFP. The mean fluorescent intensity represents LNP uptake. (**d**) NPC1$^{-/-}$ cells treated with LNP-AF647-siRNA (red) (3-h pulse, 30-min chase) and immunostained with anti-LBPA antibody (green). (**e**) LNPs containing siRNA against β integrin were added to wild-type or NPC1-deficient MEFs as in **b**, mRNA levels were quantified at 24 h after incubation using branched DNA analysis. The experiment was done in triplicate and the errors are reported as s.e.m. (**f**) A schematic representation of LNP trafficking (**i**) in NPC1$^{+/+}$ and (**ii**) NPC1$^{-/-}$ cells. Intact cationic LNPs enter through macropinocytosis (1); a small fraction of LNPs transport from macropinosomes to the endocytic recycling compartment (ERC) (2) whereas the majority is directed to late endosomes (3). Late endosome sort LNPs to lysosomes for degradation or utilize multiple recycling pathways to traffic them to the extracellular milieu. These mechanisms include recycling through transport to the ER-Golgi route (4) or direct fusion of late endosomes containing multivesicular bodies, with the plasma membrane (Exosomes secretion) (5). In NPC1-deficient cells, the late endosome recycling mechanisms are impaired, causing LNP-siRNA to accumulate in enlarged late endosomes leading to persistent escape of siRNA that improves gene silencing. (Intact nanoparticle-, siRNA complex-). All experiments were performed in triplicate. Error bars, mean ± s.e.m.

after transfection. We found an increase in the fluorescence intensity that appeared within 6 h after incubation and reached saturation at 24 h in the extracellular milieu (**Fig. 3c**). Because intact nanoparticles partially quench fluorescence from the siRNA encapsulated inside them, we exposed the supernatant to Triton-X to dissociate any intact LNPs. Exposure to Triton-X resulted in little change in fluorescence. This suggested that most LNPs had, in fact, disassembled inside cells, confirming our FRET-based data. Approximately 36% of the initial concentration of siRNA incubated with the cells recycled into the supernatant and 2.5 times (70%) the concentration of the stable siRNA was present in the supernatant relative to inside cells after 24 h (**Fig. 3d** and **Supplementary Fig. 5**).

Subcellular trafficking of lipids (e.g., cholesterol) from late endosomes and lysosomes toward the extracellular milieu has been reported to utilize the 13 transmembrane glycoprotein NPC1, which is located on the surface of multivesicular late endosomes. Absence of NPC1 causes late endosomal or lysosomal dysfunction, cholesterol accumulation and is implicated in a lysosomal storage disease that causes liver and neural degeneration in human patients and animal models[27–29]. As the components of an LNP show some similarities to the endogenous lipids that use NPC1 as a receptor for recycling, we compared LNP retention in mouse embryonic fibroblasts (MEFs) devoid of NPC1 (NPC1$^{-/-}$) with their wild-type counterparts (NPC1$^{+/+}$ MEFs) (**Fig. 4a**). NPC1-deficient cells accumulated cholesterol due to defects in recycling (**Supplementary Fig. 6**). A markedly increased level (~15-fold) of AF647-siRNA was observed in perinuclear enlarged endosomes in NPC1$^{-/-}$ compared to NPC1$^{+/+}$ MEFs at 24 h after incubation, presumably due to enhanced cellular retention at a wide range of LNP concentrations (**Fig. 4a**,**b**). Furthermore, enhanced cellular retention was observed in multiple cell types deficient in NPC1, including those isolated from human patients (**Supplementary Fig. 7a**,**b**). We further tested for differences in the kinetics of LNP

uptake in these cells. NPC1$^{-/-}$ cells had accumulated more siRNA after 2 h of incubation as compared to NPC1$^{+/+}$ cells where at early time points the amount of internalization was not affected. Moreover, a rescue experiment in which we transfected an NPC1-GFP plasmid into NPC1$^{-/-}$ cells reduced the amount of intracellular LNP-siRNA to that of wild-type cells (**Fig. 4c**, **i**,**ii**). We conclude that the greater amount of siRNA in late endosomes is based on accumulation of LNPs due to defects in constitutively active NPC1-mediated recycling. Small molecules that impair cholesterol metabolism[28] and increase cholesterol accumulation in cells failed to yield a significant increase in LNP accumulation (**Supplementary Fig. 7c**). Thus, the increased accumulation of LNPs was not due just to increased endosomal cholesterol but rather to lack of direct interaction with putative intraluminal domains of NPC1 required for egress of LNPs. NPC1$^{-/-}$ cells have been reported to have high numbers of enlarged late endosomes, containing intraluminal vesicles enriched in lysobisphosphatidic acid (LBPA)[29]. LNPs accumulated in these structures and co-localized with antibody against LBPA in these cells (**Fig. 4d**).

To study the broader potential relationship between lipid structure and NPC1-dependent LNP retention, we tested cationic siAF647-LNPs formulated with a small set of lipidoids consisting of two different amine cores, each with lipid tails of increasing chain lengths (**Supplementary Fig 11, reaction scheme**). Different LNPs containing related cationic lipids also showed increased retention in NPC1-deficient cells. We also found that increased carbon chain lengths of these cationic lipids led to better uptake and retention in both NPC1$^{+/+}$ and NPC1$^{-/-}$ MEFs (**Supplementary Fig. 8a**,**b**). This marked retention was consistent with studies that have shown that lipids with higher chain length can be inserted inside NPC1 carrying late endosome membranes[30]. Notably, liposomes containing small molecules showed similar increases in cellular retention in knockout cells (**Supplementary Fig. 8c**).

To determine whether the absence of NPC1 also leads to increased retention with polymeric nanoparticles, we tested polystyrene nanoparticles of different sizes and charges. We found a moderate increase in retention and perinuclear distribution with positively and negatively charged particles at sizes of 100 or 200 nm in NPC1$^{-/-}$ cells whereas negatively charged particles 20 nm in size (known to use a caveolae-mediated pathway[31]) showed similar retention when compared to wild-type cells (**Supplementary Fig. 8d**). We found that dextran, a marker for macropinocytosis, shows increased retention in knockout cells as compared to markers of caveolae- or clathrin-dependent endocytosis (data not shown). Thus, 20-nm particles that can access 80-nm caveolae[5,31] due to their smaller size are able to be retained inside both cell types (NPC1$^{-/-}$ and NPC1$^{+/+}$) when compared to larger particles that may only use macropinocytosis to gain entry. It is possible that macropinosomes directly fuse with NPC1-positive late endosomes and are recycled to the extracellular milieu, in the absence of which the cargo remains diverted to the endosomal-lysosomal system. It is believed that in the case of certain types of cargo, NPC1-independent recycling allows for partial escape from the endosomal-lysosomal system[30]. This may not be the case with longer chain lipids that require interaction with NPC1 for cellular exit[30]. This may be the reason for the major retention of LNPs as compared to polystyrene nanoparticles.

We hypothesized that enhanced cellular retention could translate to improved gene silencing. LNPs containing β-integrin siRNA were added to either NPC1$^{+/+}$ or NPC1$^{-/-}$ MEFs at different concentrations. A substantial improvement in LNP potency was observed in NPC1$^{-/-}$ cells in comparison to wild-type cells (**Fig. 4e**). The median inhibitory concentration ($IC_{50}$) of 1.5 nM in NPC1 deficient cells was roughly one-tenth of wild-type MEFs, and the improved potency was seen across all LNP doses tested (**Fig. 4e**). To further measure cellular retention and siRNA efficacy, NPC1$^{+/+}$ and NPC1$^{-/-}$ MEFs (stably transfected with GFP) were treated with LNPs containing GFP siRNA; high-throughput microscopy was used to simultaneously measure cellular retention and GFP fluorescence 72 h after incubation in both cell types. Enhanced cellular retention of siAF647-GFP and a decrease in normalized GFP fluorescence in NPC1$^{-/-}$compared to that in NPC1$^{+/+}$ cells were observed, confirming our previous results (**Supplementary Fig. 9a–c**). Next, we used siRNA against NPC1 to experimentally lower NPC1 protein levels in wild-type cells and a 60% reduction in protein level was achieved (**Supplementary Fig. 9d**,**e**). A fourfold increase in LNP efficacy was observed in wild-type cells treated with NPC1 siRNA when compared to the luciferase control (**Supplementary Fig. 9f**). Although this LNP efficacy was lower than what was achieved in NPC1$^{-/-}$ cells, 40% NPC1 protein still remained in NPC1$^{+/+}$ cells treated with siNPC1 and this amount may still sufficient to recycle some LNPs, albeit at a less efficient rate. The use of lipids for transfection of NPC1 siRNA may alter intracellular trafficking or recycling and further explain why these effects were partial with siRNA knockdown versus the effect seen in complete NPC1$^{-/-}$ MEFs.

This led us to further investigate which endocytic recycling pathways participate in exocytosis of LNPs, and in particular whether inhibition of these pathways could enhance cellular retention and LNP mediated gene silencing. Late endosomes have been shown to exchange material with the Golgi and endoplasmic reticulum (ER) from which the cargo can be secreted to the extracellular milieu[32,33] and/or multivesicular bodies that can fuse with the plasma membrane to release their intracellular content as exosomes[34]. Therefore, we examined the effects of siRNA that blocks secretion from the Golgi/ER (Rab8a)[32] or exosomes secretion and/or fusion with the plasma membrane (Rab27a and Rab27b)[34]. Rab8a and Rab27b siRNA treatment led to a substantial (fivefold) increase in retention of LNP in cells. A moderate increase in LNP retention was observed after reduction of Rab27a expression (**Supplementary Fig. 10a–f**). Notably, only in the case of Rab27b depletion did we detect a substantial improvement in LNP-mediated gene silencing (**Supplementary Fig. 10g**). Recent reports have shown that Rab27b inhibition leads to redistribution of late endosomes in the perinuclear region[34]. Concurrently, in our experiments both Rab27b-depleted and NPC1-deficient cells show similarly increased perinuclear retention of LNPs, which contains functional siRNA that contributes to enhanced gene silencing. On the other hand siRNA against Rab11 did not improve retention and gene silencing (**Supplementary Fig. 10h**,**i**), these results are consistent with previous reports that NPC1-mediated recycling of endogenous lipids is independent of Rab11 function even though they show some co-localization with Rab11-positive endocytic recycling compartment[35].

In summary, to enter cells, cationic LNPs require Cdc42-dependent macropinocytosis, which is shown to be regulated through $V_o$-ATPase, once internalized remain largely trapped within endosomes with little escape to the cytosol. LNP-mediated siRNA delivery can be impaired by either lack of LNP disassembly inside endosomes or their subsequent degradation in the lysosomes as well as recycling from the cell. In the absence of NPC1, due to decrease in motility of late endosomes[29], LNPs remain in enlarged late endosomes/lysosomes and are not recycled back out of the cell. One hypothesis to explain how this leads to a greater efficiency in siRNA-mediated gene silencing is that the increased residence time of more siRNA inside cells results in a slow, controlled diffusion of the siRNA into the cytoplasm

(**Fig. 4f (i,ii)**). It appears that late endosome/multivesicular late endosomes may serve as a transient reservoir where LNP recycle through multiple pathways. Prevention of direct egress of LNPs from the late endosomes leads to enhanced retention, and perinuclear positioning of these vesicular structures may serve as a persistent site for endosomal escape. Future studies that target proteins and lipids involved in biogenesis, trafficking and recycling of the late endosomes may provide further clues into the cellular factors that may improve drug delivery. Finally, the RNA-induced silencing complex (RISC) has been shown to be associated with membranes of late endosomes, and certain RISC complex components can be seen inside intraluminal vesicles of late endosomes/exosomes as well as the cytosolic side of the perinuclear rough endoplasmic reticulum[36–39]. It is possible that, in NPC1-deficient as well as Rab27b-depleted cells, LNPs remain stalled in a manner that affects siRNA delivery to RISC. From a therapeutics perspective, it is tempting to speculate that LNPs may demonstrate enhanced siRNA/drug delivery in lysosomal storage diseases where NPC1 function is impaired.

## METHODS

Methods and any associated references are available in the online version of the paper.

*Note: Supplementary information is available in the online version of the paper.*

### ACKNOWLEDGMENTS

We dedicate this work to the memory of MIT police officer Sean Collier who valiantly gave his life for the protection of the MIT community. We would like to thank P. Lobel and L. Huang from Rutgers University for NPC1 primary and immortalized cell lines. We wish to thank W. Salmon and N. Watson of the Whitehead Institute Core facility at MIT for help with confocal imaging. We would also like to thank D. Brown (Harvard MGH), K. Whitehead, R. Bogorad (MIT) and H. Yin (MIT) for healthy discussion. We would also like to thank J. Maraganore (Alnylam) and M. Invernale (MIT) for critical reading of the manuscript. Special thanks to D. Alakhova at University of Nebraska Medical Center for her help with graphic design. We would also like to thank Alnylam Pharmaceuticals, Control release grant EB000244 for funding. This work was supported by the National Heart, Lung, and Blood Institute, US National Institutes of Health, as a Program of Excellence in Nanotechnology (PEN) Award, Contract #HHSN268201000045C.

### AUTHOR CONTRIBUTIONS

G.S., R.L. and D.G.A. conceived the idea, G.S., W.Q., R.L. and D.G.A. designed research, G.S., W.Q. and C.Z. performed high-throughput microscopy. G.S., C.A., A.E., K.L., D.C. and A.S. designed LNPs and their probes, G.S., C.A., A.E., S.S. and Y.B. performed studies with NPC1 deficient and competent cells, G.S. and S.S. performed studies with autophagy based studies, G.S. and R.Z. performed TIRF microscopy, G.S. and E.K. performed systems biology, G.S., W.Q., R.L. and D.G.A. wrote the manuscript.

### COMPETING FINANCIAL INTERESTS

The authors declare competing financial interests: details are available in the online version of the paper.



1. Elbashir, S.M. *et al.* Duplexes of 21-nucleotide RNAs mediate RNA interference in cultured mammalian cells. *Nature* **411**, 494–498 (2001).
2. Whitehead, K.A., Langer, R. & Anderson, D.G. Knocking down barriers: advances in siRNA delivery. *Nat. Rev. Drug Discov.* **8**, 129–138 (2009).
3. Davis, M.E. *et al.* Evidence of RNAi in humans from systemically administered siRNA via targeted nanoparticles. *Nature* **464**, 1067–1070 (2010).
4. Sheridan, C. Proof of concept for next-generation nanoparticle drugs in humans. *Nat. Biotechnol.* **30**, 471–473 (2012).
5. Sahay, G., Alakhova, D.Y. & Kabanov, A.V. Endocytosis of nanomedicines. *J. Control. Release* **145**, 182–195 (2010).
6. Wang, J., Byrne, J.D., Napier, M.E. & DeSimone, J.M. More effective nanomedicines through particle design. *Small* **7**, 1919–1931 (2011).
7. Juliano, R.L., Ming, X. & Nakagawa, O. Cellular uptake and intracellular trafficking of antisense and siRNA oligonucleotides. *Bioconjug. Chem.* **23**, 147–157 (2012).
8. Sonawane, N.D., Szoka, F.C. Jr. & Verkman, A.S. Chloride accumulation and swelling in endosomes enhances DNA transfer by polyamine-DNA polyplexes. *J. Biol. Chem.* **278**, 44826–44831 (2003).
9. Basha, G. *et al.* Influence of cationic lipid composition on gene silencing properties of lipid nanoparticle formulations of siRNA in antigen-presenting cells. *Mol. Ther.* **19**, 2186–2200 (2011).
10. Suh, J. *et al.* Real-time gene delivery vector tracking in the endo-lysosomal pathway of live cells. *Microsc. Res. Tech.* **75**, 691–697 (2012).
11. Lu, J.J., Langer, R. & Chen, J. A novel mechanism is involved in cationic lipid-mediated functional siRNA delivery. *Mol. Pharm.* **6**, 763–771 (2009).
12. Nguyen, J. & Szoka, F.C. Nucleic acid delivery: the missing pieces of the puzzle? *Acc. Chem. Res.* **45**, 1153–1162 (2012).
13. Collinet, C. *et al.* Systems survey of endocytosis by multiparametric image analysis. *Nature* **464**, 243–249 (2010).
14. Doherty, G.J. & McMahon, H.T. Mechanisms of endocytosis. *Annu. Rev. Biochem.* **78**, 857–902 (2009).
15. Chen, D. *et al.* Rapid discovery of potent siRNA-containing lipid nanoparticles enabled by controlled microfluidic formulation. *J. Am. Chem. Soc.* **134**, 6948–6951 (2012).
16. Love, K.T. *et al.* Lipid-like materials for low-dose, in vivo gene silencing. *Proc. Natl. Acad. Sci. USA* **107**, 1864–1869 (2010).
17. Leuschner, F. *et al.* Therapeutic siRNA silencing in inflammatory monocytes. *Nat. Biotechnol.* **29**, 1005–1010 (2011).
18. Zoncu, R. *et al.* mTORC1 senses lysosomal amino acids through an inside-out mechanism that requires the vacuolar H(+)-ATPase. *Science* **334**, 678–683 (2011).
19. Carette, J.E. *et al.* Ebola virus entry requires the cholesterol transporter Niemann-Pick C1. *Nature* **477**, 340–343 (2011).
20. Khalil, I.A., Kogure, K., Akita, H. & Harashima, H. Uptake pathways and subsequent intracellular trafficking in nonviral gene delivery. *Pharmacol. Rev.* **58**, 32–45 (2006).
21. Huss, M. *et al.* Concanamycin A, the specific inhibitor of V-ATPases, binds to the V(o) subunit c. *J. Biol. Chem.* **277**, 40544–40548 (2002).
22. Bayer, N. *et al.* Effect of bafilomycin A1 and nocodazole on endocytic transport in HeLa cells: implications for viral uncoating and infection. *J. Virol.* **72**, 9645–9655 (1998).
23. Ravikumar, B. *et al.* Regulation of mammalian autophagy in physiology and pathophysiology. *Physiol. Rev.* **90**, 1383–1435 (2010).
24. Sarkar, S. *et al.* Complex inhibitory effects of nitric oxide on autophagy. *Mol. Cell* **43**, 19–32 (2011).
25. Akinc, A. *et al.* Targeted delivery of RNAi therapeutics with endogenous and exogenous ligand-based mechanisms. *Mol. Ther.* **18**, 1357–1364 (2010).
26. Alabi, C.A. *et al.* FRET-labeled siRNA probes for tracking assembly and disassembly of siRNA nanocomplexes. *ACS Nano* **6**, 6133–6141 (2012).
27. Ikonen, E. Cellular cholesterol trafficking and compartmentalization. *Nat. Rev. Mol. Cell Biol.* **9**, 125–138 (2008).
28. Ko, D.C., Gordon, M.D., Jin, J.Y. & Scott, M.P. Dynamic movements of organelles containing Niemann-Pick C1 protein: NPC1 involvement in late endocytic events. *Mol. Biol. Cell* **12**, 601–614 (2001).
29. Zhang, M. *et al.* Cessation of rapid late endosomal tubulovesicular trafficking in Niemann–Pick type C1 disease. *Proc. Natl. Acad. Sci. USA* **98**, 4466–4471 (2001).
30. Koivusalo, M., Jansen, M., Somerharju, P. & Ikonen, E. Endocytic trafficking of sphingomyelin depends on its acyl chain length. *Mol. Biol. Cell* **18**, 5113–5123 (2007).
31. Lai, S.K., Hida, K., Chen, C. & Hanes, J. Characterization of the intracellular dynamics of a non-degradative pathway accessed by polymer nanoparticles. *J. Control. Release* **125**, 107–111 (2008).
32. Linder, M.D. *et al.* Rab8-dependent recycling promotes endosomal cholesterol removal in normal and sphingolipidosis cells. *Mol. Biol. Cell* **18**, 47–56 (2007).
33. Stenmark, H. & Olkkonen, V.M. The Rab GTPase family. *Genome Biol.* **2**, REVIEWSS3007 (2001).
34. Ostrowski, M. *et al.* Rab27a and Rab27b control different steps of the exosome secretion pathway. *Nat. Cell Biol.* **12**, 19–30 (2010).
35. Hölttä-Vuori, M., Tanhuanpää, K., Möbius, W., Somerharju, P. & Ikonen, E. Modulation of cellular cholesterol transport and homeostasis by Rab11. *Mol. Biol. Cell* **13**, 3107–3122 (2002).
36. Gibbings, D.J., Ciaudo, C., Erhardt, M. & Voinnet, O. Multivesicular bodies associate with components of miRNA effector complexes and modulate miRNA activity. *Nat. Cell Biol.* **11**, 1143–1149 (2009).
37. Lee, Y.S. *et al.* Silencing by small RNAs is linked to endosomal trafficking. *Nat. Cell Biol.* **11**, 1150–1156 (2009).
38. Siomi, H. & Siomi, M.C. RISC hitches onto endosome trafficking. *Nat. Cell Biol.* **11**, 1049–1051 (2009).
39. Stalder, L. *et al.* The rough endoplasmatic reticulum is a central nucleation site of siRNA-mediated RNA silencing. *EMBO J.* **32**, 1115–1127 (2013).

## ONLINE METHODS

**Cell culture.** All cell types were grown in DMEM/10% FBS, including (i) HeLa cells—wild type, stable cells that co-express Luciferase and Renilla (Dual HeLa) or GFP—were provided by Alnylam Pharmaceuticals. (ii) NPC1 immortalized MEFs ($NPC^{+/+}$ and $NPC^{-/-}$) or primary MEFs ($NPC^{-/-}$, $NPC^{-/+}$, $NPC^{+/+}$) were kind gifts from P. Lobel at Rutgers University. (iii) NPC1-deficient human patient fibroblasts and age-matched NPC1 competent control were obtained from Coriell Institute of Medical Research. (iv) $Atg5^{+/+}$ and $Atg5^{-/-}$ cells were provided by Sovan Sarkar (Rudolph Jaenisch laboratory, MIT). (v) Stably transfected LLC-PK1 epithelial tubulin-GFP cell line were kind gifts from D. Brown of Massachusetts General Hospital, Boston.

**Endocytosis markers and small molecule library.** *Plasmid DNA*. Cdc42-GFP construct (Origene), Arf6-GFP construct (Origene), Traffic light LC3-GFP-mRFP construct and NPC1-GFP (provided by Sovan Sarkar, Rudolph Jaenisch laboratory, MIT), Rab7-GFP, Rab11-GFP and dominant negative DNRab11-GFP (provided by Roberto Zoncu, from David Sabatini's laboratory at MIT), Rab5-RFP inside baculovirus (Life Technologies) were used for transfections in HeLa cells. Small-molecule library was purchased from Enzo Life Sciences and concanamycin, imipramine, fluphenazine and U18666A were obtained from Sigma Aldrich. *Endocytic tracers*. AF (Alexa Fluor) 594 Transferrin (Life Technologies) and AF 594 Ovalbumin (Life Technologies), Lysotracker Red (Life Technologies) were used as markers for select endocytic vesicles in HeLa cells. *Antibodies*. Mouse Anti Lysosomal Associate Membrane Protein-1 (LAMP1 Developmental Studies Hybridoma Bank; 1:200, H4A3), Mouse Anti Lysosomal Associated Membrane Protein-2 (LAMP2, Santa Cruz; 1:200, H4B4), Mouse anti-LBPA (lysobisphosphatidic acid, Echleon Biosciences; 1:100, 6C4), Mouse anti-EEA1 (BD Transduction; 1:50, 14/EEA-1), Mouse Anti-Rab11 (BD Transduction; 1:500, A-11008/A10680). Goat anti-mouse Alexa Fluor 488 IgG antibody was used as a secondary antibody (Life Technologies).

**siRNA.** *Purchased from Dharmacon.* (a) **siRNA NPC1 pool (purchased from Dharmacon)- siNPC1-09-CGGACAGAGCUUCGCGAAU, siNPC1-10-CCUUGAAUGAUACGAGUUU, siNPC1-11-ACAUAGGGCCGUCGGUGAA, siNPC1-12-GGGAGUGACUACCGCGUAU**. (b) siRNA Rab 11 pool (purchased from Dharmacon)-siRab11-7-GCAACAAUGUGGUUUCCUAU, siRab11-8-CAAGAGCGAUAUCGAGCUA, siRNA-9-GUGCAGUGCUGUCAGAACA (most efficacious, data not shown), siRNA-10-GAGAUUUACCGCAUUGUUU

*Provided by Alnylam Pharmaceuticals*. (2′-OMe modified nucleotides are in lower case and phosphorothioate linkages are represented by 's'):

a. siRNA Alexa Fluor 647 (siAF647GFP). GFP sense: AcAuGAAGcAGcACGACuUdTsdT

GFP antisense: AAGUCGUGCUGCUUCAUGUdTdT-Alexa-Fluor-647

b. siRNA Luciferase LUC sense: cuuAcGcuGAGuAcuucGAdTsdT

LUC antisense: UCGAAGuACUcAGCGuAAGdTsdT

c. Cdc 42 siRNA: CGGAAUAUGUACCGACUGU

d. Rac1 siRNA: GUGAUUUCAUAGCGAGUUU

e. Clathrin Heavy Chain (CHC): GCAGAAGAAUCAACGUUAU

f. Caveolin-1 (Cav-1):GCAUCAACUUGCAGAAAGA

g. siRNA against β-integrin was provided by Alnylam and Roman Bogorad, MIT. Sense: AGAuGAGGuucAAuuuGAAdTsdT

Antisense:

UUcAAAUUGAACCUcAUCUdTsdT

*Silencer Select Validated siRNA purchased from Ambion (Life Technologies).*

a. Rab8a- Sense:GCAAGAGAAUUAAACUGCAtt, Antisense:UGCAGUUUAAUUCUCUUGCca

b. Rab27a-Sense GCCUCUACGGAUCAGUUAAtt Antisense:UUAACUGAUCCGUAGAGGCat

c. Rab27b- Sense GACUUAAUCAUGAAGAGAAtt Antisense:UUCGCUUCAUGAUUAAGUCca

Life Technologies GAPDH siRNA was validated and used as a control.

*FRET probe*. siRNA duplexes labeled at the 5′ end of the sense strand with either Alexa Fluor 594 or Alexa Fluor 647 dyes were purchased from Integrated DNA Technologies. Sense 5′-AF594-GAUUAUGUCCGGUUAUGUAUU-3′, 5′-AF647-GAUUAUGUCCGGUUAUGUAUU-3′ and antisense 5′-UACAUAACCGGACAUAAUCUU-3′.

**Nanoparticles preparation.** *Lipid nanoparticles.* Cationic LNPs were prepared by rapidly mixing equal volumes of an ethanol solution of lipidoid and aqueous solution of siRNA on a microfluidic device, followed by dilution by PBS buffer[15]. The lipidoid solution contained C12-200 (ref. 16) or lipidoids consisting of two different amine cores, each with lipid tails of increasing chain lengths[15] (new cationic lipids tested have been reported in the reaction scheme shown below), cholesterol (Avanti Polar Lipids), distearoyl phosphatidylcholine (DSPC, Avanti Polar Lipids), and a polyethylene glycol modified lipid ((*R*)-3-[(ω-methoxy-PEG2000-carbamoyl)]-1,2-di-*O*-tetradecyl-*sn*-glyceride ($mPEG_{2000}$-DMG; synthesized by Alnylam, Cambridge, MA as previously described[25]) solubilized in 90% ethanol at mass concentrations of C12-200 (2.0 mg/ml); DSPC (0.28 mg/ml); cholesterol (0.52 mg/ml); $mPEG_{2000}$-DMG (0.13 mg/ml). The siRNA was dissolved in 10 mM citrate, pH 3.0 buffer at a concentration of 0.4 mg/ml. To prepare LNPs, the siRNA solution, the lipidoid solution, and PBS buffer were injected into a microfluidic mixing device at volumetric flow rates of siRNA (300 liters/min); lipids (300 liters/min); buffer (600 liters/min), using three syringes (Gastight syringes, Hamilton Company), which were controlled by two syringe pumps (PHD 2000, Harvard Apparatus). Ethanol was removed by dialyzing LNPs against PBS buffer using membranes with MWCO of 3.5 kD (PierceProtein Research). In the case of liposomes designed to carry small molecules, hydrogenated soybean phosphatidylcholine (HSPC; Avanti Polar Lipids) was dissolved in ethanol and hydrated in a 5% dextrose solution with 0.2 mg/ml Alexa Fluor 647 (AF647) hydrazide tris(triethylammonium) salt (Molecular Probes) at 52 °C to form multilamellar vesicles (MLV). The MLV were downsized to form small unilamellar vesicles (SUV) by stepwise extrusion through polycarbonate membranes (SterliTech) using a Lipex extruder (Northern Lipids) starting at a pore diameter of 400 nm and ending at 100 nm. Nonencapsulated dye was removed by dialysis. LNPs generated through microfluidics were around 100 nm in size; the physicochemical properties of these nanoparticles have been previously characterized[15].

**Polystyrene fluospheres.** Polystyrene nanoparticles of different sizes and charge—negatively charged were carboxylate modified (200 nm, 100 nm and 20 nm), positively charged were amine modified (200 nm)—were purchased from Life Technologies (Carlsbad).

**Confocal microscopy.** *High-throughput confocal microscopy.* HeLa-GFP cells were seeded at $1.5 \times 10^4$ cells per well in black 96-well plates (Greiner Bio-one). Cells were pulsed with 50 nM of lipid nanoparticle (C12-200) encapsulated with Alexa Fluor 647 siRNA (siAF647-LNP) for 3 h, cells were washed, chased for multiple time points (0 min, 5 min, 15 min, 30 min and 60 min), fixed and counterstained with Hoechst. In select experiments to study the effect of small molecules on cellular uptake, cells were first pre-incubated for 30 min (or 24 h for cholesterol modulators) with the small molecules at a concentration of 10 μM (concentration for bafilomycin and concanamycin were kept at 1 μM and 500 nM, respectively). The cells were then incubated with siAF647 LNP for 3 h, washed and fixed after 60-min chase. For determination of subcellular localization of LNPs, HeLa cells (3 h pulse, 0–60 min chase) were fixed, permeabilized with 0.05% saponin and incubated with antibodies against LAMP1, LAMP2, Rab11, EEA1 for 2 h in room temperature or 24 h at 4 °C, washed, and followed by addition of secondary antibody for staining. In case of experiments that require transfection of plasmid DNA, cells were transfected (Lipofectamine 2000) 24 h before addition of LNPs. Furthermore, experiments that required treatment with Lysotracker (100 nM) or transferrin (5 μg/ml) were conducted with addition of these markers in the last 30 min of the 3 h LNP incubation period, followed by similar processing as discussed above. High-throughput microscopy was also conducted on $NPC1^{+/+}$ and $NPC1^{-/-}$ that were plated in the same 96-well plates (half plate each), for simultaneous visualization and quantification of LNP retention (as well as GFP silencing) with equal exposure. In select experiments $NPC1^{-/-}$ cells exposed to LNPs (3 h pulse, 30-min chase) were subjected to permeabilization and incubation with anti-LBPA followed by detection using a secondary antibody. In all experiments cells were then counterstained in OPTI-MEM containing Hoechst

(2 μg/ml) for nuclei identification. Triple-stained live cell imaging was done with an automated spinning disk confocal microscope (OPERA, Perkin Elmer) with a 40× objective. Vesicles containing LNPs are pseudo-colored red whereas vesicles containing endocytic markers were pseudo-colored green, unless otherwise stated. The same defined pattern of 20 fields from each well was acquired to eliminate bias and provide a statistically significant number of cells for analysis. After identification of cell location and perimeter, intracellular siRNA signal intensity and in select cases GFP fluorescence was calculated over single field using Acapella software. Data represent intracellular intensity from 20 different fields. For quantitative co-localization of LNPs with endocytic markers a script was prepared that measures multiple parameters including the overall percent co-localization of two different spots. All experiments were done in triplicate and errors were plotted as standard error of the mean (s.e.m.). *High-resolution confocal microscopy.* 50,000 HeLa cells/well were plated in chambered glass coverslips and allowed to grow for 1 d. Similar pulse (3 h) and chase (0, 15, 30, 60 min) experiments with LNP (50 nM) were conducted as mentioned above. Cells were fixed and permeabilized (0.05% saponin) followed by addition of primary antibodies and secondary antibodies. For localization studies based on overexpression of endocytic markers or other controls, plasmid DNA was transfected 24 h before addition of LNPs. The cells were washed with PBS and imaged (63×) using a Perkin Elmer Spinning Disk Confocal Microscope. A z-stack was taken using the volocity software and an extended z-focus has been presented for **Figure 2b** (in most cases, like **Fig. 2c**, the image quantification is done using high-throughput microscopy, unless otherwise stated, in which case Image-J software was used). The three-dimensional z-stack for untreated cells and bafilomycin-treated cells was constructed using the Imaris Software. *TIRF microscopy.* Cells were imaged using TIRF microscopy as previously described[18]. Briefly, HeLa-GFP cells were incubated with LNPs for 3 h in presence or absence of bafilomycin (1 μM). The cells were washed and imaged at 37 °C using a Nikon spinning disk confocal microscope with an objective fitted with a 60× objective for 15 or 30 min. TIRF microscopy lens was controlled by an Andor iQ software. Cells were typically imaged in two channels by sequential excitation at 0.25 Hz or 0.5 Hz, without binning, with 200 or 500 ms exposures and detected with an EMCCD camera. The depth of the evanescent field was 100 nm. Cells were typically imaged with Alexa Fluor 647 (far red) channels and GFP (green) channel. The GFP serves as a control, which shows that the microscope retained stable focus of the membrane in focus during time-lapse imaging experiments (data not shown) whereas the Alexa Fluor 647 channel showed dynamic punctate structures indicative of endosomal vesicles. Movies were made using Image-J software; **Supplementary Movie 1** represents membrane level LNP trafficking whereas **Supplementary Movie 2** is representative of LNP trafficking in the presence of bafilomycin.

**Multiple particle tracking. Supplementary Movies 1** and **2** were subjected to multiple particles tracking using the Imaris software. An algorithm based on Autoregression motion model was applied to each movie. Spots/vesicles detected via Imaris Tracker were further processed by setting a threshold for spot detection based on visual accuracy of the predicted spots; a sphere was applied to represent each vesicle (8 μm). A gap size of 3 μm and maximum distance of 15 μm were set for prediction of the movement of a given spot to its next subsequent time point. The tracks were then filtered based on the accuracy of vesicular motion; the color-coded tracks (based on track duration) represent overall movement of each vesicle. The statistical values like track displacement and track duration were exported and the ratio of average values generated for **Supplementary Movies 1** and **2** were calculated.

**Systems analysis.** The protein-protein and protein–small molecule interaction networks were constructed using the GeneGo Metacore platform. Proteins of interest were imported and subnetworks around the proteins were created with an 'auto-expand' algorithm. The auto-expand algorithm gradually expanded subnetworks around every object from the list of imported proteins. Connectivity is directional (to and from the initial object), and both directions were considered separately. Expansion was halted when the subnetworks intersected, or when the overall network size reached some pre-established limit of 100. The networks were then exported to Cytoscape[40] for further analysis and visualization of the final networks. Clusters around the small molecules of interest were identified based on the node connectivity. To identify the functionality of the gene clusters, we assigned Gene Ontology attributes to the networks. To assign Gene Ontology attributes we used the BiNGO algorithm[41] within the Cytoscape platform. It is important to note that molecules that caused >10–15% toxicity were not included for systems analysis.

**FRET assay.** HeLa cells were washed with a 10% growth media in PBS solution and resuspended in 0.5 ml of 10% growth media in PBS. The cells were sieved with a cell strainer (BD Bioscience) before flow cytometry analysis. 10,000 events were monitored and evaluated by a BD LSR II HTS flow cytometer (BD Bioscience). A 561-nm (yellow-green) excitation laser was used to excite the Alexa Fluor (AF) 594 fluorophore and its emission was observed with a 610/20-nm filter. A 633-nm (red, HeNe) laser was used to excite the AF647 fluorophore and its emission was observed with a 660/20-nm filter. Each channel was compensated for bleed through using single-fluorophore controls. FRET was monitored by exciting the samples with a 561-nm excitation laser and observing their emission with a 695/40-nm emission filter set. Data points represent an average of duplicate experiments. For stability assays FRET studies were done in the presence or absence of bafilomycin in OPTI/MEM. In select experiments LLC-PK1 epithelial tubulin-GFP cells were treated with LNP-FRET probe for 3 h, washed and imaged 1 h after incubation; individual fluorophores were imaged. AF647 signal: pseudo-colored green; AF594 signal: pseudo-colored red; tubulin-GFP signal: pseudo-colored gray.

**Fluorescence-activated cell sorting (FACS)/flow cytometry.** After aspirating conditioned medium, cells were washed with PBS and detached with 0.25% trypsin-EDTA (25 μl, Life Technologies). FACS running buffer (50 μl), consisting of 98% PBS and 2% FBS, was added to each well. Cells were mixed thoroughly and then transferred to a 96-well round-bottom plate, and the AF647 signal was measured by FACS on a BD LSR II equipped with a fluid-handling robot (Becton Dickinson, San Jose, CA, USA). Cell gating and analysis were performed using FlowJo v8.8 software (TreeStar, Ashland, OR, USA). For transfection experiments involving GFP fusion proteins, GFP signal was collected in addition to the AF647 signal; two-dimensional gating was used to separate increased auto-fluorescence signals from increased GFP signals, and in these experiments transfected cells within the top 25th percentile of GFP expression were considered positive for significant transgene expression. Cell gating and analysis were done using FlowJo v8.8 software (TreeStar, Ashland, OR, USA).

**Stable cells generation.** Replication-incompetent lentiviral particles containing the GFP ORF were packaged in 293T cells with a VSV-G coat and used to infect MEFs. Virus-containing supernatant was collected 48, 60 and 72 h after transfection. 2 μg/ml of polybrene was added and the supernatant was filtered through a 0.45-μm filter and used for the infection. Culture medium (DMEM supplemented with 10% FBS (Hyclone), penicillin/streptomycin, L-glutamine and nonessential amino acids) was changed 12 h after the last infection.

**siRNA transfection.** *β-integrin siRNA transfection.* 50,000 NPC1 $^{+/+}$ or NPC1$^{-/-}$ were plated in 24-well plates. LNPs (C12-200/siβ-integrin) were added to cells grown overnight at different dilutions (the final concentration of siRNA in cells ranged from, 1.5–50 nM in OPTI-MEM). The cells were washed after 3 h and replenished with complete media. The cells were lysed after 24 h and B-DNA assay was performed. C12-200/ siLUC containing LNP (50 nM) served as a positive control. In select experiments wild-type cells treated with siNPC1 twice (as discussed below) were further treated with LNP (siβ-integrin) followed by B-DNA assay after 24 h. A similar experiment was performed with Atg5$^{+/+}$ and Atg5$^{-/-}$ cells. *NPC1 siRNA transfection.* NPC1$^{+/+}$ MEFs were exposed to siRNA against NPC1 (0.1–10 nM) using Lipofectamine RNA interference (RNAi) Max in serum-free media (OPTI-MEM). siRNA against luciferase serve as a negative control. The cells were lysed at 24 h for B-DNA assay and 72 h for western blot analysis. In select experiments cells were retransfected (48 h after first transfection) for achievement of complete silencing of NPC1 followed by western blot analysis after 48 h (96 h of reverse transfection). *siRNA to silence endocytic regulators.* siRNA against Cdc42, Rac1, CHC, Cav-1, Rab11 were validated (data not shown). The most efficacious




doi:10.1038/nbt.2614

siRNA was transfected to HeLa cells using Lipofectamine RNAi Max (50 nM, 6 h). After 48 or 72 h, the cells were retransfected with the lipid/siRNA complex (50 nM, 3 h) and the cells were exposed to siAF647-LNPs (50 nM, 3 h) after 24 h. The cells were fixed, counterstained with Hoechst and subjected to high-throughput confocal microscopy. *siRNA to silence late endocytic recycling regulators.* siRNA against Rab8a (10 nM), Rab27a (10 nM), Rab28b (10 nM), GAPDH (10 nM) and Rab11 (50 nM, twice) were validated (data not shown). siRNA was transfected to Dual HeLa cells using Lipofectamine RNAi Max for 6 h, cells were washed and their media replaced. After 72 h the cells were exposed to siAF647-LNPs (50 nM, 3 h); cells were washed and incubated with fresh media for 3 h then fixed, counterstained with Hoechst and subjected to high-throughput confocal microscopy. In case of efficacy studies the (siRab) pretreated cells (post 72 h) were transfected with siLuc-LNP (0.15, 1.5, 15 and 150 nM). Relative firefly luciferase silencing was assessed 24 h after transfection using a Dual-Glo luciferase assay kit (Promega, Madison, WI). Normalization to Renilla luciferase values served as a control for potential toxicity. *Western blot analysis.* Cell pellets were lysed on ice in Laemmli buffer (62.5 mM Tris-HCl pH 6.8, 2% SDS, 5% β-mercaptoethanol, 10% glycerol and 0.01% bromophenol blue) for 30 min in the presence of complete protease inhibitor cocktail (Roche Diagnostics), boiled for 5–7 min at 100 °C and subjected to western blot analysis, as previously described[24]. Primary antibodies include anti-NPC1 and anti-actin (kind gifts from Sovan Sarkar at Rudolph Jaenisch laboratory). Blots were probed with anti-mouse or anti-rabbit IgG-HRP secondary antibody (1:4,000 dilutions) and visualized using ECL detection kit (GE Healthcare).

**Branched-DNA (B-DNA) assay.** HeLa cells treated with LNPs were lysed in cell lysis buffer (Epicenter) containing Proteinase K. The Quantigene assay 2.0 (Affymetrix, previously Panomics) was used to measure mRNA knockdown (β-integrin or NPC1) according to manufacturer's instructions. Levels of the target gene were compared to a known housekeeping gene GAPDH and then normalized to controls.


40. Shannon, P. *et al.* Cytoscape: a software environment for integrated models of biomolecular interaction networks. *Genome Res.* **13**, 2498–2504 (2003).
41. Maere, S., Heymans, K. & Kuiper, M. BiNGO: a Cytoscape plugin to assess overrepresentation of gene ontology categories in biological networks. *Bioinformatics* **21**, 3448–3449 (2005).